Journal of Magnetic Resonance 209 (2011) 359–363

Contents lists available at ScienceDirect

Journal of Magnetic Resonance

journal homepage: www.elsevier.com/locate/jmr

Communication

Heteronuclear dipolar decoupling in solid-state nuclear magnetic resonance under ultra-high magic-angle spinning

Venus Singh Mithu [a], Subhradip Paul [a], Narayanan D. Kurur [b], P.K. Madhu [a,*]

[a] Department of Chemical Sciences, Tata Institute of Fundamental Research, Homi Bhabha Road, Colaba, Mumbai 400 005, India
[b] Department of Chemistry, Indian Institute of Technology Delhi, Hauz Khas, New Delhi 110 016, India

ARTICLE INFO

Article history:
Received 4 December 2010
Revised 24 January 2011
Available online 15 February 2011

Keywords:
Solid-state NMR
Heteronuclear dipolar decoupling
Magic-angle spinning
TPPM
SPINAL
PISSARRO
Swept-frequency TPPM

ABSTRACT

We compare in this communication several heteronuclear dipolar decoupling sequences in solid-state nuclear magnetic resonance experiments under a magic-angle spinning frequency of 60 kHz. The decoupling radiofrequency field amplitudes considered are 190 and 10 kHz. No substantial difference was found among the sequences considered here in performance barring the difference in the optimisation protocol of the various schemes, an aspect that favours the use of swept-frequency two pulse phase modulation (SW_f-TPPM).

1. Introduction

In solid-state nuclear magnetic resonance (NMR), in order to improve the resolution and sensitivity of rare spins, such as ^{13}C and ^{15}N, dipolar coupled to the abundant spins, such as ^{1}H, efficient heteronuclear dipolar radiofrequency (RF) pulse schemes need to be applied on the ^{1}H channel [1]. Some of the prominent decoupling schemes currently used are TPPM [2], SPINAL [3], XiX [4,5], and SW_f-TPPM [6]. A crucial aspect in the field of decoupling is the ease of setting up of the sequences besides the sensitivity and resolution advantages. SW_f-TPPM has been found to perform better than the other methods either in terms of sensitivity or robustness with respect to experimental parameters or both in decoupler amplitude regimes of more than 50 kHz and magic-angle spinning (MAS) frequencies of 5–30 kHz [7–11].

Under rotary-resonance (RR) conditions, when the decoupler RF frequency is an integral multiple of the MAS frequency $\nu_1 = n\nu_r$ ($n = 1,2,\ldots$) [12], decoupling despite recoupling is accomplished by either PISSARRO [13] or high-phase TPPM schemes [14]. PISSARRO was also shown to accomplish decoupling at off-RR conditions at high MAS of 60 kHz and low decoupler RF amplitudes of 15 kHz although its efficiency was only compared with the continuous-wave decoupling on the ^{1}H channel [15].

Feasibility of MAS at frequencies up to 70–80 kHz has led to considerations such as: The possibility of decoupling at very low RF amplitudes (e.g. 15 kHz), comparison of the efficiency of the various schemes at low RF amplitudes, magnitude of the decoupling RF amplitude required for various schemes at the high-amplitude regime, and the comparison of various schemes at high RF amplitudes. There have been a few reports in this direction exploring decoupling at MAS frequencies of 40–50 kHz and RF amplitudes down to 13–15 kHz [16–19].

We report in this communication the performance efficiency of TPPM, SPINAL, SW_f-TPPM, XiX, and PISSARRO schemes at a MAS frequency of 60 kHz and two decoupling RF amplitudes of 190 and 10 kHz. It is observed that in this extreme regime of MAS frequency, irrespective of the high or low RF amplitude, all the schemes behave in a similar way with regard to the decoupling efficiency. We present here experimental results on a sample of U–^{13}C-L-glycine and U–^{13}C-L-histidine·HCl·H_2O at the ^{1}H Larmor frequency of 600 MHz.

2. Experimental

The experiments were carried out on a BRUKER AVIII 600 MHz spectrometer equipped with a 1.3 mm triple-resonance probe. The experiments were done on commercially purchased U–^{13}C-L-glycine and U–^{13}C-L-histidine·HCl·H_2O without any further purification. A sample of commercially available adamantane was used for the calibration of RF amplitude via nutation experiments.

* Corresponding author. Fax: +91 22 2280 4610.
E-mail address: madhu@tifr.res.in (P.K. Madhu).

1090-7807/$ - see front matter © 2011 Elsevier Inc. All rights reserved.
doi:10.1016/j.jmr.2011.01.028

3. Results and discussions

Fig. 1 shows the intensity of the $^{13}CH_2$ peak of U–^{13}C-L-glycine for the different sequences at the MAS frequency (ν_r) of 60 kHz and at RF amplitudes (ν_1) of 10 kHz and 190 kHz. For the different sequences the pulse length at $\nu_1 = 10$ kHz was optimised in the following manner:

(a) SW$_f$-TPPM, TPPM, and SPINAL-64: The pulse length τ_p was optimised by varying τ_p in the range corresponding to a flip angle of 140–220°. The optimum pulse length was found to be in the vicinity of the value corresponding to 180°. The phase for each of these sequences was also optimised. For TPPM and SW$_f$-TPPM the optimal phase for each unit of $\tau_\phi\ \tau_{-\phi}$ was found to be $\phi = 15°$. The SPINAL-64 used here is of the form $Q\overline{Q}Q\overline{Q}Q\overline{Q}Q\overline{Q}$, where $Q \equiv \tau_\phi\tau_{-\phi}$, $\tau_{\phi+5}\tau_{-\phi-5}$, $\tau_{\phi+10}\tau_{-\phi-10}$, $\tau_{\phi+5}\tau_{-\phi-5}$, where the optimal value of ϕ was found to be same as that of TPPM.

(b) PISSARRO and XiX: The recommended pulse length for these two sequences are in the region $\nu_1\tau_p = k2\pi$ [15,17]. For optimisation of pulse length, it was varied over a range which corresponds to a flip angle variation of ±40° around the conditions $\nu_1\tau_p = k2\pi$, ($k = 1,2$). The optimal flip angle was in the vicinity of 360°.

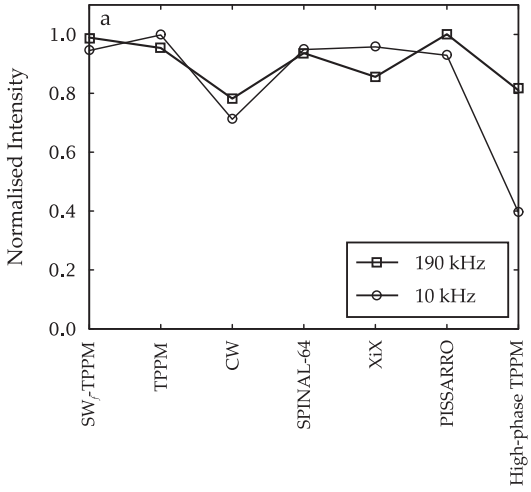

Fig. 1. Intensity of the $^{13}CH_2$ peak of U–^{13}C-L-glycine obtained with different heteronuclear dipolar decoupling sequences at $\nu_1 = 10$ kHz and $\nu_1 = 190$ kHz at $\nu_r = 60$ kHz. The intensities are normalised to the best intensity obtained with PISSARRO.

The pulse length optimisation for the high RF amplitude of $\nu_1 = 190$ kHz was done in the following fashion:

(a) SW$_f$-TPPM, TPPM and SPINAL-64: The pulse length τ_p was optimised by varying τ_p in the range corresponding to a flip angle of 140–220°. The optimum pulse lengths for the three sequences correspond to 188°, 185°, and 170° respectively. The optimal phase values are same as that used at $\nu_1 = 10$ kHz.

(b) PISSARRO: The optimum pulse length at high RF amplitude was found to be at $\tau_p = 0.93\tau_r$.

(c) XiX: The recommended pulse length for XiX at high RF amplitude is $2.85\tau_r$ [5]. The experimentally optimised pulse length for best decoupling here was at $\tau_p = 2.65\tau_r$.

From Fig. 1 it can be concluded that TPPM performs the best at the low RF amplitude but the sequences SW$_f$-TPPM, SPINAL-64, XiX, and PISSARRO deliver almost the same intensity and all of the aforementioned sequences are within 90% of the best intensity obtained. All of these sequences perform much better than CW as expected. High-phase TPPM is designed to work at the $n = 1,2,\ldots,$RR conditions and hence yields a poor decoupling efficiency at the experimental conditions considered here. In the regime of high RF amplitude decoupling at high MAS frequencies PISSARRO and SW$_f$-TPPM deliver the best performance whilst TPPM and SPINAL-64 deliver 95% and 92% of the best intensity obtained respectively followed by XiX, high-phase TPPM, and CW. The intensities are normalised with respect to the best intensity obtained with PISSARRO.

We now investigate the robustness of the aforementioned sequences towards experimental parameters like the pulse length and the offset on ^{1}H. Fig. 2 shows the offset dependence at both high and low RF amplitudes of (a) $\nu_1 = 10$ kHz and (b) $\nu_1 = 190$ kHz at $\nu_r = 60$ kHz. The carrier frequency was varied in the range of ±6 kHz from the centre of the proton resonance of glycine and the intensity of the $^{13}CH_2$ peak is monitored as a function of the proton offset. From Fig. 2a and b it can be inferred that all the sequences show similar offset dependence but at $\nu_1 = 10$ kHz, the offset dependence becomes much more critical as at ±6 kHz offset the intensity drops to almost 20% of the best intensity obtained using TPPM. From these two plots it can be concluded that at low RF amplitudes the offset dependence is much more critical. The best intensity is obtained at ~2 kHz as it is the on-resonance position for the $^{13}CH_2$ peak relative to the centre of the proton spectra of glycine.

Fig. 3 shows the pulse length dependence of the various sequences at $\nu_1 = 10$ kHz and $\nu_r = 60$ kHz. The optimal pulse length

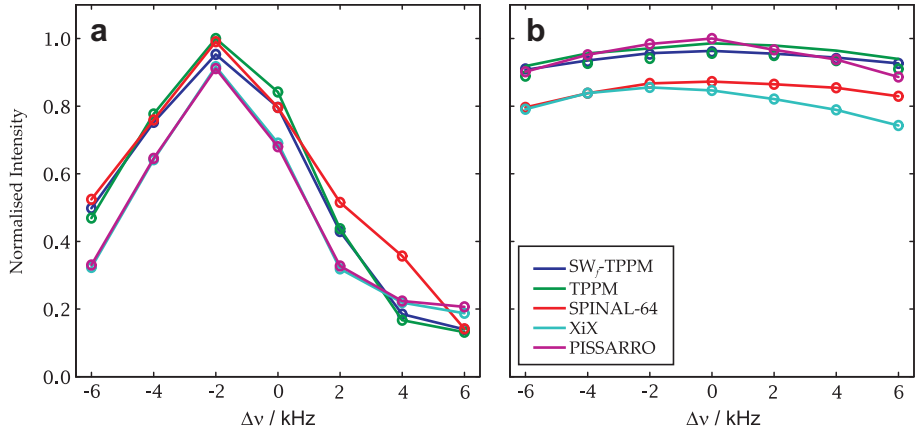

Fig. 2. Intensity of the $^{13}CH_2$ peak of U–^{13}C-L-glycine as a function of offset on ^{1}H at (a) $\nu_r = 60$ kHz and $\nu_1 = 10$ kHz, and (b) $\nu_r = 60$ kHz and $\nu_1 = 190$ kHz. The intensities are normalised to the best intensity obtained with (a) TPPM and (b) PISSARRO.

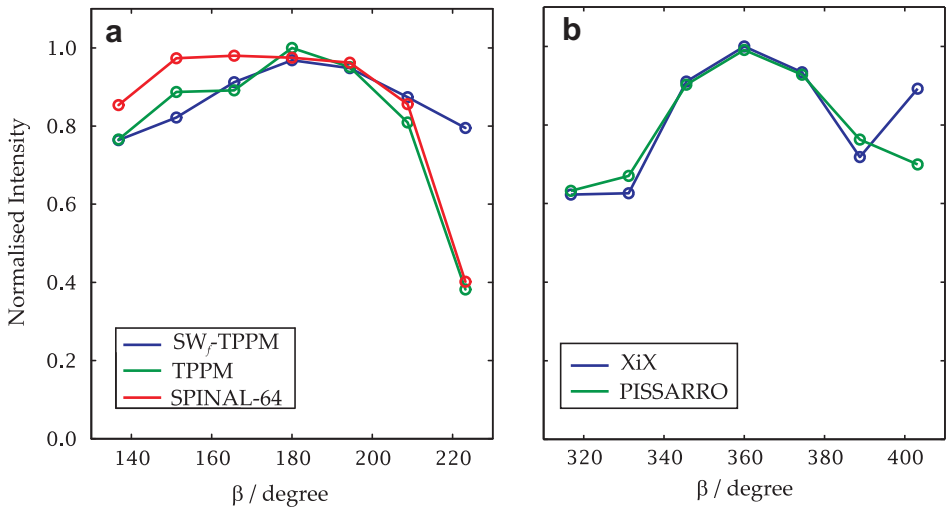

Fig. 3. Intensity of the $^{13}CH_2$ peak of U–^{13}C-L-glycine as a function of flip angle (β) corresponding to the decoupling pulse of length τ on ^{1}H at ν_r = 60 kHz and ν_1 = 10 kHz. The pulse lengths were optimised around (a) $\nu_1\tau_p \approx \pi$ for TPPM, SW$_f$-TPPM, and SPINAL-64 and (b) $\nu_1\tau_p \approx 2\pi$ for XiX and PISSARRO over a range of ±40° with respect to (a) π and (b) 2π.

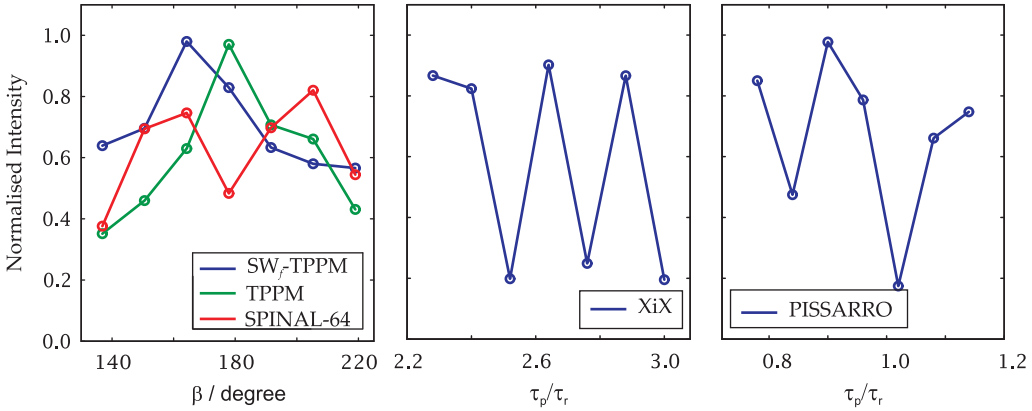

Fig. 4. Intensity of the $^{13}CH_2$ peak of U–^{13}C-L-glycine as a function of pulse length for (a) TPPM, SW$_f$-TPPM, and SPINAL-64, (b) XiX and (c) PISSARRO. For (a) the pulse lengths were optimised over a range of ±40° around the pulse length corresponding to a flip angle of 180°. For (b) the pulse length was varied over a range of 2.3–3.0τ_r whilst for (c) it was varied in the range of 0.7–1.2τ_r.

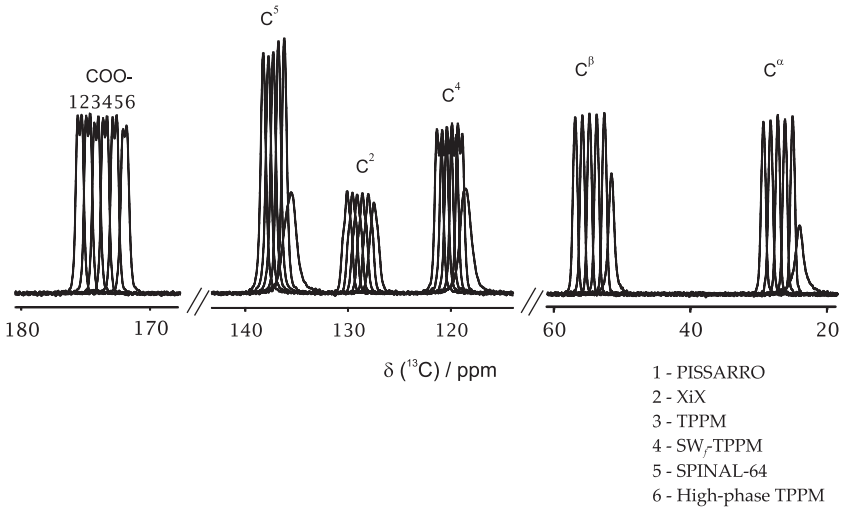

Fig. 5. $^{13}CH_2$ (C^α) and ^{13}CH (C^β), aromatic region (C^2, C^4, and C^5), and carbonyl resonance of U–^{13}C-L-histidine·H_2O at ν_1 = 10 kHz and ν_r = 60 kHz. The chemical-shift axis corresponds to the spectra obtained with SW$_f$-TPPM. The three regions have been scaled horizontally by different magnitudes for clarity.

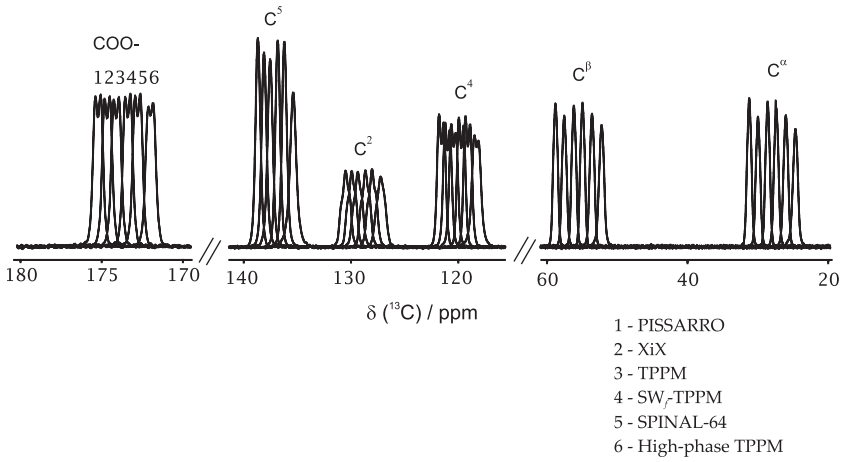

Fig. 6. $^{13}CH_2$ (C^{α}) and ^{13}CH (C^{β}), aromatic region (C^2, C^4, and C^5), and carbonyl resonance of U–^{13}C-L-histidine·H_2O at ν_1 = 190 kHz and ν_r = 60 kHz. The chemical-shift axis corresponds to the spectra obtained with SW_f-TPPM. The three regions have been scaled horizontally by different magnitudes for clarity.

for TPPM, SW_f-TPPM, and SPINAL-64 should correspond to a flip angle around 180° whilst that for XiX and PISSARRO should correspond to multiples of 360°. We varied the flip angle in the range of ±40° around these optimal values. Comparing Fig. 3a and b it can be concluded that SPINAL and SW_f-TPPM show slightly better performance as compared to the other decoupling sequences in terms of pulse length.

Fig. 4 shows the pulse length dependence of these sequences at high RF amplitude, ν_1 = 190 kHz. The optimal pulse length for TPPM, SW_f-TPPM, and SPINAL-64 should correspond to a flip angle around 180° whilst that for XiX is around $2.85\tau_r$ and for PISSARRO in the regime of $0.9\tau_r$ to $1.1\tau_r$ [5,15]. In order to optimise the pulse lengths we varied it in the range corresponding to ±40° of 180° for TPPM, SW_f-TPPM, and SPINAL-64 in Fig. 4a. For XiX we varied the pulse length in the range of $0.1\tau_r$ to $3.5\tau_r$ but here we show the region from $2.2\tau_r$to $3\tau_r$. For PISSARRO we varied the pulse length in the range of $0.1–3.0\tau_r$, with a subset from 0.75 to $1.15\tau_r$ shown in Fig. 4c. From the three plots it can be concluded that TPPM and SW_f-TPPM are the most forgiving sequences in terms of pulse length misset whilst XiX and PISSARRO are least forgiving to this parameter.

We have applied TPPM, SW_f-TPPM, SPINAL-64, XiX, and PISSARRO on U–^{13}C-L-histidine·HCl·H_2O in order to investigate their decoupling efficiency on a sample having a wide spread of proton resonance frequencies. Fig. 5 shows the $^{13}CH_2$ (C^{α}) and ^{13}CH (C^{β}), aromatic region (C^2, C^4, and C^5), and carbonyl resonance of the ^{13}C spectra of U–^{13}C-L-histidine·H_2O at ν_1 = 60 kHz and ν_r = 10 kHz. From the three plots it can be concluded that all of these sequences deliver almost the same decoupling efficiency with SW_f-TPPM and SPINAL-64 marginally better than the other sequences. Fig. 6 shows the same at ν_1 = 190 kHz. At the high RF amplitude regime PISSARRO and SW_f-TPPM seem to perform slightly better than the other sequences in terms of intensity of different peaks.

4. Conclusions

We have presented here a comparison study of different heteronuclear decoupling sequences at high MAS frequency of 60 kHz and at RF amplitudes of 190 kHz and 10 kHz. The results show that the decoupling efficiency of these sequences are almost the same at both the regimes of the RF amplitude indicating that high MAS does the primary averaging. Differences among these decoupling schemes in the T_2 values [21] is currently being investigated.

The parameters for optimisation are different for XiX and PISSARRO under different regimes of MAS frequency and RF amplitude. A careful optimisation of TPPM and SPINAL also requires a multiparameter fit. We have found that the performance of SW_f-TPPM has only a marginal dependence on the pulse duration and the phase angle. The pulse duration for SW_f-TPPM can be normally kept at the value corresponding to a flip angle of 180° and the phase value can be set at ϕ = ±15° for all ranges of MAS frequency and RF amplitude. Hence, use of SW_f-TPPM is still favourable over the other schemes for all routine purposes. This fact was presumably made use of in a study involving a protein by the group of Emsley where SW_f-TPPM was used at low RF amplitudes under high MAS [20]. It was particularly mentioned that SW_f-TPPM achieves decoupling over a broader bandwidth compared to TPPM. This feature of SW_f-TPPM would be crucial in the investigation of complicated systems, such as proteins.

Acknowledgments

P.K.M. acknowledges assistance from Department of Science and Technology, India, for funding under SERC scheme, SR/S1/PC/27/2009. We acknowledge the National Facility for High Field NMR, TIFR, Mumbai, and technical assistance of M.V. Naik. We also acknowledge Prof. C.L. Khetrapal and Dr. Neeraj Sinha, Center of Biomedical Magnetic Resonance, Lucknow, India, for providing us the facility to perform the experiments.

References

[1] M. Ernst, Heteronuclear spin decoupling in solid-state NMR under magic-angle sample spinning, J. Magn. Reson. 162 (2003) 1.
[2] A.E. Bennet, C.M. Rienstra, M. Auger, K.V. Lakshmi, R.G. Griffin, Heteronuclear decoupling in rotating solids, J. Chem. Phys. 103 (1995) 6951.
[3] B.M. Fung, A.K. Khitrin, K. Ermolaev, An improved broadband decoupling sequence for liquid crystals and solids, J. Magn. Reson. 142 (2000) 97.
[4] P. Tekely, P. Palmas, D. Canet, Effect of proton spin exchange on the residual ^{13}C MAS NMR linewidths. Phase-modulated irradiation for efficient heteronuclear decoupling in rapidly rotating solids, J. Magn. Reson. A107 (1994) 129.
[5] A. Detken, E.H. Hardy, M. Ernst, B.H. Meier, Simple and efficient decoupling in magic-angle spinning solid-state NMR: the XiX scheme, Chem. Phys. Lett. 356 (2002) 298.
[6] R.S. Thakur, N.D. Kurur, P.K. Madhu, Swept-frequency two-pulse phase modulation for heteronuclear dipolar decoupling in solid-state NMR, Chem. Phys. Lett. 426 (2006) 459.
[7] M. Leskes, R.S. Thakur, P.K. Madhu, N.D. Kurur, S. Vega, Bimodal Floquet description of heteronuclear dipolar decoupling in solid-state nuclear magnetic resonance, J. Chem. Phys. 127 (2007) 024501.
[8] R.S. Thakur, N.D. Kurur, P.K. Madhu, An analysis of phase-modulated heteronuclear dipolar decoupling sequences in solid-state nuclear magnetic resonance, J. Magn. Reson. 193 (2008) 77.
[9] R.S. Thakur, N.D. Kurur, P.K. Madhu, Pulse Duration and Phase Modulated Heteronuclear Dipolar Decoupling Schemes in Solid-state NMR, in: Proc. of Ind. Nat. Sci. Acad., Springer Verlag, 2010.

[10] S. Paul, N.D. Kurur, P.K. Madhu, On the choice of heteronuclear dipolar decoupling scheme in solid-state NMR, J. Magn. Reson. 207 (2010) 140.
[11] C.V. Chandran, P.K. Madhu, N.D. Kurur, T. Bräuniger, Swept-frequency two-pulse phase modulation (SW_f-TPPM) sequences with linear sweep profile for heteronuclear decoupling in solid-state NMR, Magn. Reson. Chem. 46 (2008) 943.
[12] T.G. Oas, R.G. Griffin, M.H. Levitt, Rotary resonance recoupling of dipolar interactions in solid-state nuclear magnetic resonance spectroscopy, J. Chem. Phys. 89 (1988) 692.
[13] M. Weingarth, P. Tekely, G. Bodenhausen, Efficient heteronuclear decoupling by quenching rotary resonance in solid-state NMR, Chem. Phys. Lett. 466 (2008) 247.
[14] S. Paul, V.S. Mithu, N.D. Kurur, P.K. Madhu, Heteronuclear dipolar decoupling in solid-state nuclear magnetic resonance at rotary resonance ronditions, J. Magn. Reson. 203 (2010) 199.
[15] M. Weingarth, P. Tekely, G. Bodenhausen, Low-power decoupling at high spinning frequencies in high static fields, J. Magn. Reson. 199 (2009) 238.
[16] M. Ernst, A. Samoson, B.H. Meier, Low-power decoupling in fast magic-angle spinning NMR, Chem. Phys. Lett. 348 (2001) 293.
[17] M. Ernst, A. Samoson, B.H. Meier, Low-power XiX decoupling in MAS NMR experiments, J. Magn. Reson. 163 (2003) 332.
[18] X. Filip, C. Tripon, C. Filip, Heteronuclear decoupling under fast MAS by a rotor-synchronized Hahn-echo pulse train, J. Magn. Reson. 176 (2005) 239.
[19] M. Kotecha, N.P. Wickramasinghe, Y. Ishii, Efficient low-power heteronuclear decoupling in ^{13}C high-resolution solid-state NMR under fast magic angle spinning, Magn. Reson. Chem. 45 (2007) S221.
[20] J.R. Lewandowski, J. Sein, H.J. Sass, S. Grzesiek, M. Blackledge, L. Emsley, Measurement of site-specific ^{13}C spin-lattice relaxation in a crystalline protein, J. Am. Chem. Soc. 132 (2010) 8252.
[21] G. De Paëpe, N. Giraud, A. Lesage, P. Hodgkinson, A. Böckmann, L. Emsley, Transverse dephasing optimized soid-state NMR spectroscopy, J. Am. Chem. Soc. 125 (2003) 13938.